Bayesian Recursive Estimation on the Rotation Group

Sofia Suvorova[1], Stephen D Howard [2], and Bill Moran[1]

[1]Department of Electrical and Electronic Engineering, University of Melbourne, Parkville, Australia
Email: sofia.suvorova@unimelb.edu.au, wmoran@unimelb.edu.au
[2]Defence Science and Technology Group, Edinburgh, Australia
Email: Stephen.Howard@dsto.defence.gov.au

***Abstract*—Tracking on the rotation group is a key component of many modern systems for estimation of the motion of rigid bodies. To address this problem, here we describe a Bayesian algorithm that relies on directional measurements for tracking on the special orthogonal (rotation) group. Its novelty lies in the use of maximum entropy distributions on these groups as models for the priors, and justifiable approximation algorithms that permit recursive implementation of such a model. We provide the solutions in a recursive closed form. In the two-dimensional case the parameters of the prior and posterior distributions can be computed exactly and the solution has low complexity. Adoption of this approach eliminates the problem of angle wrapping. In higher dimensions the exact solution cannot be computed, and it is necessary to make (very close) approximations, which is done here. We demonstrate in simulations that, in contrast with some other approaches, our algorithm produces very accurate and statistically meaningful outputs.**

I. Introduction

Recursive estimation of the orientation of moving rigid bodies or jointed systems of rigid bodies is an important problem in many areas of application. For instance, this problem arises for spacecraft navigation, satellite control and space junk estimation [1]–[5], estimation of robot configurations [6]–[11], and in tracking of human and animal body motions [12]–[16]. Such problems arise wherever at least part of the dynamics of the system under observation can be characterised as preserving distance from a fixed centre, or in the case of jointed systems from multiple (relatively) fixed centres. By removing linear motion of the centre of mass of the rigid body via estimation by, say, a Kalman Filter, quite general rigid body and jointed body motions can be modelled in terms of rotations. A mathematically and statistically correct model for these problems represents dynamical changes in the system in terms of elements of the group $\mathcal{SO}(N)$ of rotations on $\mathbb{R}^N$ where, in cases of practical interest, $N = 2,\ 3$. We focus mainly on those two dimensions here. Uncertainty about these dynamical changes of state, and of the state itself, are appropriately expressed in terms of probability distributions on $\mathcal{SO}(N)$. Tracking in this context, then, requires a method for updating that representation, taking into account measurements that provide probabilistic information about the state.

The choice of a family of distributions to represent the uncertainty is always problematic once one departs from the linear Gaussian model on $\mathbb{R}^N$, where the Kalman filter, using Gaussian noise models, is demonstrably optimal for natural measures of performance. Several approaches to the tracking of rotations rely on linear approximations both to the state space $\mathcal{SO}(N)$ and to the dynamical model (see [7], [17], [18]). Other approaches use linear estimation methods to undertake recursive rotation estimation where rotations are sometimes represented by quaternions [19]–[21]. For this formulation, the additive Gaussian noise assumption of the Kalman filter is inappropriate simply because the addition of Gaussian noise to a rotation matrix will not, in general, result in another rotation matrix. Accordingly, these methods need to use some way of "projecting" the results back into the correct manifold. In practice, as a result of the ill-fitting model for the noise, these algorithms usually require very frequent re-initialization of the tracker.

The Complementary Filter as described in [22]–[24] overcomes the above problems to some degree, but does not provide a mechanism for computing error parameters. In effect, it is a constant gain filter and, as a result, only *ad hoc* internal methods for correction of the tracker are available.

There are many rationales for using the linear Gaussian models in $\mathbb{R}^N$, not least of which is that it accords well with physical reality in many situations. However, the "process noise" aspect of the linear Gaussian model is typically chosen because it is an easily computable distribution to represent uncertainty about the actual dynamical process. This choice is justified, in the absence of knowledge of the process noise distribution, because the Gaussian is the maximal entropy distribution on $\mathbb{R}^N$ with a given covariance matrix. It is, in effect, the distribution that makes minimal assumptions about the statistics of noise beyond that its covariance matrix is given. The corresponding maximal entropy distributions on the rotation group [25]–[29] have densities with respect to the (invariant) Haar measure of the form

$$\mathcal{VMF}(\mathbf{R}|\mathbf{W}) = \Lambda(\mathbf{W})e^{\mathrm{Tr}(\mathbf{WR})}, \quad \{\mathbf{R} \in \mathcal{SO}(N)\}, \quad (1)$$

where $\mathbf{W}$ is a given $N \times N$ matrix, and $\Lambda(\mathbf{W})$ is a normalizing factor such that

$$\int_{\mathcal{SO}(N)} \mathcal{VMF}(\mathbf{R}|\mathbf{W})\, \mathrm{d}\nu(\mathbf{R}) = 1. \quad (2)$$

Here $\mathrm{d}\nu(\mathbf{R})$ is the (left and right invariant) Haar measure on the special rotation group [30] (Sec 15-16). The distributions in

(1) are called matrix *von Mises-Fisher distributions* and have been widely studied [26], [28], [29], [31]–[35]. The matrix $\mathbf{W}$ encompasses both a "rotational modal" matrix, corresponding to the mean in the Gaussian case; and a "concentration" matrix as a measure of spread playing the role of a covariance matrix in the Gaussian case. Bayesian recursive estimation on the circle, using a similar formalism is found in the recent work in [36]. A three dimensional case is handled with an unscented filter in [37].

The class of von Mises-Fisher matrix distributions has the pleasing and useful property that the (pointwise) product of two densities of this kind is also the density (up to normalization) of a von Mises-Fisher matrix distribution, since

$$e^{\mathrm{Tr}(\mathbf{W}_1\mathbf{R})}e^{\mathrm{Tr}(\mathbf{W}_2\mathbf{R})} = e^{\mathrm{Tr}[(\mathbf{W}_1+\mathbf{W}_2)\mathbf{R}]}. \tag{3}$$

However, dynamical updates via Bayes' Rule, or more specifically, via the ChapmanKolmogorov equation, of a given von Mises-Fisher distribution based on, say, a constant angular velocity model, do not typically retain the von Mises-Fisher character. Thus, the linear equivariance of the linear Gaussian model, a key aspect of the exactness of the Kalman filter, fails for such distributions as it does for many linear tracking schemes that do not strictly accord with the conditions for the Kalman filter. As in the linear case, when this happens, an approximation scheme is needed to project back into this class in order to produce a recursive filter. We describe such a scheme in this paper. We strongly emphasise that, in our case, we are projecting a *distribution on the rotation group* into a particular class of such distributions; we are not projecting a *state outside the rotation group* into the rotation group as, for instance, linear approximation methods do. A different approach for such an approximation is investigated in [38] for the problem of multiple scattering on the hypersphere. One desirable character of our scheme is that it always produces a spread that is no better (that is more uncertain) than is the case for the unapproximated distribution. This is an important property: this filter effectively assumes no more than is given by the underlying model and the observations. This contrasts with other approaches and, especially, with the extended Kalman filter (EKF).

This paper is the first of two on this work. The focus here is on development of the theory and the generic algorithm. A second paper will focus on more practical aspect of the tracker, including the pseudo-code and experiments with the real Inertial Measurement unit (IMU) data.

We first describe a filter in the case when $N = 2$ in Section II. In this simpler case the method is precise. The more difficult case of a $\mathcal{SO}(3)$ and the appropriate approximations, along with some numerical experiments, are described in Section III. Our conclusion follows. As we have stated, experimental results using real measurements are deferred to a later paper.

II. Tracking on $\mathcal{SO}(2)$

We begin with the simpler case of tracking on $\mathcal{SO}(2)$. In applications this might apply, for instance, to the tracking of the phase of a sinusoidal signal or of the position of an object rotating on a fixed axis. This problem and our approach to it are illustrative of the 3-dimensional case (and indeed higher dimensional cases), but have significant differences, in dimensions greater that 2 we have to resort to approximations that are less strict, though at least in three dimensions well justified.

A key difference between the 2-dimensional and the higher dimensional situations is that the group $\mathcal{SO}(2)$ is commutative, whereas higher dimensional rotations groups are not. In the 2-dimensional situation, the angular statistics are modelled by a classical von Mises distribution. For simplicity, the measurements of direction (angle) are also assumed in our work here to be distributed according to a von Mises distribution, though that is not essential for the method. Indeed more general measurement regimes are easily accommodated. We show that, under a mild assumption, a Kalman-like filter can be found to achieve effective tracking. The von Mises distribution on the circle is the maximal entropy distribution for a given mean direction and concentration. Using this as our model prior, our approach is to find the best von Mises distribution that incorporates the measurement after calculation of the posterior. Most importantly, whatever "best" means it should not produce a distribution that makes more assumptions than are warranted by the data. The *von Mises distribution* on $\mathcal{SO}(2)$ is given by the probability density function

$$\mathcal{VM}(r|\hat{r},\kappa) = \frac{1}{2\pi I_0(\kappa)}\exp[\kappa\cos(r-\hat{r})], \tag{4}$$

where I_0 is a zeroth order modified Bessel function of the first kind, and $\hat{r}$ and κ are the mean direction and concentration parameters of the distribution, respectively. The parameters $\hat{r}$ and κ play similar roles to the mean and variance in a normal distribution. To be more specific, the moments of the von Mises distribution are usually calculated as the moments of $z = \exp(ir)$ rather than the angle r itself (see [39]). The first moment of z is

$$\hat{z} = \int_{-\pi}^{\pi} e^{ir}\mathcal{VM}(r|\hat{r},\kappa)\,\mathrm{d}r = \frac{I_1(\kappa)}{I_0(\kappa)}\exp(i\hat{r}). \tag{5}$$

In this case $\hat{r} = \arg\hat{z}$ is defined to be the *circular mean* of r, the variance of z is the *circular variance* for r; that is,

$$\sigma = 1 - |\hat{z}| = 1 - \frac{I_1(\kappa)}{I_0(\kappa)}. \tag{6}$$

The concentration κ is recovered by inverting Equation (6). For faster computation, the inversion is approximately computed by replacing σ by an upper bound (again erring on the side of weaker assumptions) as found in [40], producing

$$\kappa = \left[(\sigma-1) + \frac{1}{\sigma-1}\right]^{-1}. \tag{7}$$

We describe a recursive solution to this problem using von Mises pdfs in Sections II-A, followed by a numerical example in Section II-B.

A. Problem formulation and algorithm

Our objective, here, is to estimate the parameters of the posterior distribution of an angle r (given by Equation (4)) of the rotation about a fixed point, relative to a fixed axis on a plane, using a given sequence of noisy measurements of r acquired at discrete times t_k, $k = 1, \ldots, K$. The measurements are denoted by $x_0, \ldots, x_K$, and the sequence of measurements up and including t_k by $X^{(k)} = (x_0, \ldots, x_k)$. The measurement noise is captured by the noise concentration parameters $\eta_0, \ldots, \eta_K$.

The evolution of r from the $(k-1)$th to the kth epochs — the *process noise* in the system — is assumed here to be given by a random rotation p, also modelled by a von Mises distribution with known mean p_k and concentration κ_{p_k}; in other words, a random walk on the circle (at least in the maximum entropy view).

An alternative process noise model useful for many applications, would involve a specification of the dynamics in terms of ω— an angular velocity distribution rather than a random walk on a circle. The angular velocity distribution, being on the tangent space $\mathbb{R}$, is appropriately modelled by in terms of a Gaussian with mean $\hat{\omega}$ and variance v^2:

$$\mathcal{N}(\omega|\hat{\omega}, v) = \frac{1}{v\sqrt{2\pi}} \exp\left[-\frac{(\omega - \hat{\omega})^2}{2v^2}\right]. \tag{8}$$

For $\mathcal{SO}(2)$ for small errors the Gaussian measurement distribution on the tangent space to the circle at $\hat{\omega}$ can be approximated by the von Mises $\mathcal{VM}(\omega|\hat{\omega}, \kappa)$. The parameters κ and v^2 are related through the expansion

$$\kappa \cos(\omega - \hat{\omega}) = \kappa - \frac{\kappa}{2}(\omega - \hat{\omega})^2 + O\left[(\omega - \hat{\omega})^4\right]. \tag{9}$$

That is, we take

$$\kappa = v^{-2}. \tag{10}$$

For a time between epochs denoted as Δt, the parameters of the process noise distribution are

$$\begin{aligned} p_k &= \hat{\omega}\Delta t, \\ \kappa_{p_k} &= (v\Delta t)^{-2}. \end{aligned} \tag{11}$$

Here we give the solution for the case of the random walk on the circle. The random angular velocity case is treated similarly. In the three dimensional context, described in Section III we discuss both of the corresponding cases in detail.

a) Initialization: The distribution for r at time $k = 0$ is taken to be a $\mathcal{VM}(r|x_0, \eta_0)$.

b) Prediction: Let the posterior distribution of r at time $1 \leq k$ be given by the mean r_{k-1} and concentration $\kappa_{r_{k-1}}$; that is,

$$\mathrm{f}(r|X^{(k-1)}) = \frac{\exp[\kappa_{r_{k-1}} \cos(r - r_{k-1})]}{2\pi I_0(\kappa_{r_{k-1}})}. \tag{12}$$

Under the random walk dynamics regime, the the orientation of the object changes by a random rotation angle p also assumed to follow a $\mathcal{VM}(p|p_k, \kappa_{p_k})$. The orientation at time k is predicted to be $\exp(ir)\exp(ip) = \exp[i(r+p)]$, where the probability density of the predicted value of the angle $q = r+p$ is a convolution of the densities of p and r:

$$\begin{aligned} \mathrm{f}(q|X^{(k-1)}) &= \frac{1}{4\pi^2 I_0(\kappa_{r_{k-1}}) I_0(\kappa_{p_k})} \\ &\times \int_{-\pi}^{\pi} \exp[\kappa_{r_{k-1}} \cos(r - r_{k-1}) + \kappa_{p_k} \cos(q - r - p_k)]\, \mathrm{d}r. \end{aligned} \tag{13}$$

The distribution of $p+r$ is no longer von Mises and to remain in the von Mises regime, we use Equation (5) to calculate the circular mean and variance of q

$$\begin{aligned} \int_{-\pi}^{\pi} \mathrm{f}(q|X^{(k-1)}) \exp(iq)\, \mathrm{d}q = \frac{I_1(\kappa_{r_{k-1}})}{I_0(\kappa_{r_{k-1}})} \frac{I_1(\kappa_{p_k})}{I_0(\kappa_{p_k})} \times \\ \exp[i(r_{k-1} + p_k)]. \end{aligned} \tag{14}$$

This yields

$$\begin{aligned} \text{circular mean:} \quad & q_k = r_{k-1} + p_k \\ \text{circular variance:} \quad & \sigma_{q_k} = 1 - \frac{I_1(\kappa_{r_{k-1}})}{I_0(\kappa_{r_{k-1}})} \frac{I_1(\kappa_{p_k})}{I_0(\kappa_{p_k})} \\ & = 1 - (1 - \sigma_{r_{k-1}})(1 - \sigma_{p_k}), \\ \text{concentration :} \quad & \kappa_{q_k} = \left[(\sigma_{q_k} - 1) + \frac{1}{\sigma_{q_k} - 1}\right]^{-1}, \end{aligned} \tag{15}$$

where κ_{q_k} is computed via Equation (7). We now "project back" to a von Mises distribution using these values for the circular mean and concentration to obtain the prior distribution of r at k'the epoch:

$$\mathrm{f}(r|X^{(k-1)}) = \frac{1}{2\pi I_0(\kappa_{q_k})} \exp[\kappa_{q_k} \cos(r - q_k)]. \tag{16}$$

c) Update: It is assumed here that the angular measurements x_k are also instances of a von Mises distribution with mean r and concentration η_k. That is, the measurement likelihood is

$$\mathcal{L}(x_k|r) = \frac{1}{2\pi I_0(\eta_k)} \exp[\eta_k \cos(x_k - r)]. \tag{17}$$

By Bayes' Rule the posterior distribution of r at time k is

$$\begin{aligned} \mathrm{f}(r|X^{(k-1)}) &\propto \mathcal{L}(x_k|r)\, \mathrm{f}(r|X^{(k-1)}) \\ &= \exp[\eta_k \cos(x_k - r) + \kappa_{q_k} \cos(r - q_k)]. \end{aligned} \tag{18}$$

The new, updated mean r_k and concentration κ_{r_k} of r can be computed exactly from Equation (18), as the phase and magnitude of $\eta_k e^{ix_k} + \kappa_{q_k} e^{iq_k}$

$$\begin{aligned} r_k &= \arctan\Big[\frac{\eta_k \sin(x_k) + \kappa_{q_k} \sin(q_k)}{\eta_k \cos(x_k) + \kappa_{q_k} \cos(q_k)}\Big], \\ \kappa_{r_k} &= \sqrt{\eta_k^2 + \kappa_{q_k}^2 + 2\eta_k \kappa_{q_k} \cos(x_k - q_k)}. \end{aligned} \tag{19}$$

The posterior distribution of r at time t_k is

$$\mathrm{f}(r|X^{(k-1)}) = \frac{1}{2\pi I_0(\kappa_{r_k})} \exp[\kappa_{r_k} \cos(r - r_k)]. \tag{20}$$

Equations (15), (16), (19) and (20) together now provide a complete procedure for recursive estimation in this context.

B. Numerical example

The algorithm is illustrated with an example of tracking an object which moves on a circle with a constant velocity of 0.1 rad/s clockwise by measuring its angle with the y-axis. In this example, the angle measurement is simulated every second with noise concentration parameter $\eta = 1$ (dimensionless). The filter parameters for the dynamics are: $\hat{p} = 0.1$ rad/s and $\kappa_p = 10$.

For comparison the tracking is performed both by a Kalman filter (since the dynamic and the measurement equations are linear) and the $\mathcal{SO}(2)$-tracker described here. What is important for our purposes is to test the ability of the method to deal with the periodic nature of angles by analysing the behaviour of the tracker near the "break points" $\pm\pi$ rad. While our approach deals with this issue automatically, since the parameter being tracked is on the circle, the Kalman filter fails to track as it is unable to handle apparently large "jumps" in measurements. This is illustrated in Figure 1. We note that it would be relatively straightforward to fix this problem in the Kalman filter by shifting the phase or unwrapping the measurements, but our method is both simple and natural, and does not require any heuristic "tweaking" of this kind.

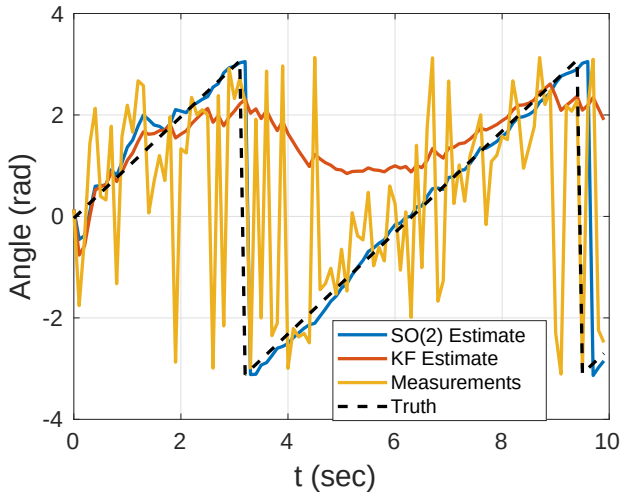

Fig. 1. *Example: $\mathcal{SO}(2)$ vs. Kalman Filter Tracking*

III. Tracking on $\mathcal{SO}(3)$

Now we turn to the much more difficult three dimensional case. Our aim is the same as in the two dimensional case: to compute the posterior distribution of a rotating object. Here, the object under observation is rotating in three dimensions and its orientation is represented by an element of the rotation group

$$\mathcal{SO}(3) = \{\mathbf{R} \in \mathcal{O}(3) | \det(\mathbf{R}) = 1\}. \tag{21}$$

We provide a recursive solution to this problem in Section III-A. Numerical examples are presented in Section III-B.

The maximal entropy probability distributions on $SO(3)$ are the *von Mises-Fisher* matrix distributions. More precisely, given a specified "mean" 3×3 matrix $\mathbf{Z}$, the von Mises-Fisher distributions are solutions to the optimization problem:

$$\mathrm{f}_Z(\mathbf{R}) = \mathrm{argmax}_{\mathrm{f}} \Big\{ \int_{\mathcal{SO}(3)} \log \mathrm{f}(\mathbf{R}) [\mathrm{d}\mathbf{R}] : \int_{\mathcal{SO}(3)} \mathbf{R}\, \mathrm{f}(\mathbf{R})\, \mathrm{d}\nu(\mathbf{R}) = \mathbf{Z} \Big\}. \tag{22}$$

The maximum entropy condition forces $\mathrm{f}_Z(\mathbf{R})$ to be of the form $\mathcal{VMF}(\mathbf{R}|\mathbf{W})$:

$$\mathcal{VMF}(\mathbf{R}|\mathbf{W}) = \Lambda(\mathbf{W})^{-1} e^{\mathrm{Tr}(\mathbf{W}\mathbf{R})}, \qquad \mathbf{R} \in \mathcal{SO}(3), \tag{23}$$

where the matrix $\mathbf{W} \in \mathbb{R}^{3\times 3}$ of rank ≥ 2 is chosen to satisfy

$$\mathbb{E}(\mathbf{R}) = \int_{\mathcal{SO}(3)} \mathbf{R} \mathcal{VMF}(\mathbf{R}|\mathbf{W})\, \mathrm{d}\nu(\mathbf{R}) = \mathbf{Z}, \tag{24}$$

where $\mathrm{d}\nu(\mathbf{R})$ is normalized Haar measure, providing the invariant integral on $\mathcal{SO}(3)$, so that

$$\int_{\mathcal{SO}(3)} \mathrm{d}\nu(\mathbf{R}) = 1. \tag{25}$$

The normalizing constant $\Lambda(\mathbf{W})$ for the von Mises-Fisher distribution in (23) is given by

$$\Lambda(\mathbf{W}) = \int_{\mathcal{SO}(3)} e^{\mathrm{Tr}(\mathbf{W}\mathbf{R})}\, \mathrm{d}\nu(\mathbf{R}). \tag{26}$$

It is important to note that, for the full orthogonal group $\mathcal{O}(3)$, the corresponding integral to (26), which in reality is $\frac{1}{2}[\Lambda(\mathbf{W}) + \Lambda(-\mathbf{W})]$, is the well-known hypergeometric function (of the eigenvalues) of $\mathbf{W}$, ${}_0F_1(\frac{3}{2}; \frac{1}{4}\Sigma^2)$, as shown in [26]–[29]. However, to the best of our knowledge, properties of the normalizing constant $\Lambda(\mathbf{W})$ for the case of the *special* orthogonal group $\mathcal{SO}(3)$, have not been studied in detail.

In Appendix A we provide the framework for the angle-axis representation of rotations in $\mathcal{SO}(3)$, required to proceed with computations of the $\mathcal{SO}(3)$ tracker. In Appendix B we describe an asymptotic expansion of $\Lambda(\mathbf{W})$ in terms of the eigenvalues of $\mathbf{W}$.

a) Polar decomposition: For our purposes, an important representation of the matrix $\mathbf{W}$ is its *polar decomposition*, as a product of a polar and an elliptical component [25]; that is,

$$\mathbf{W} = \hat{\mathbf{R}}^T \mathbf{A}, \tag{27}$$

where the polar component $\hat{\mathbf{R}}$ is a member of $\mathcal{SO}(3)$ and $\mathbf{A}$ is symmetric. We give a specific definition of these next. Regarded as the *modal* and *concentration* matrices of the distribution, they are analogous to the circular mean and concentration in $\mathcal{SO}(2)$ case. Following [41], to obtain $\hat{\mathbf{R}}$ and $\mathbf{A}$, we start with the singular value decomposition of $\mathbf{W}$:

$$\mathbf{W} = \mathbf{U}\Sigma\mathbf{V}^T, \tag{28}$$

where

$$\Sigma = \mathrm{diag}(s_1, s_2, s_3), \tag{29}$$

organised so that $s_1 \geq s_2 \geq s_3 \geq 0$, and $\mathbf{U}$ and $\mathbf{V}$ are orthogonal matrices with

$$\det(\mathbf{V}\mathbf{U}^T) = \pm 1. \tag{30}$$

Now we define

$$\mathbf{D} = \mathrm{diag}(1, 1, \det(\mathbf{V}\mathbf{U}^T)), \tag{31}$$

and write

$$\begin{aligned} \hat{\mathbf{R}} &= \mathbf{V}\mathbf{D}\mathbf{U}^T \\ \mathbf{A} &= \mathbf{V}\mathbf{D}\Sigma\mathbf{V}^T. \end{aligned} \tag{32}$$

The resulting $\hat{\mathbf{R}}$ is forced to belong to $\mathcal{SO}(3)$. This is our polar decomposition.

b) Approximation with von Mises-Fisher distribution: As in the $\mathcal{SO}(2)$ case, the probability distribution of the predicted rotation in $\mathcal{SO}(3)$ tracker is "projected back" to a von Mises-Fisher (maximum entropy) distribution. This raises the issue of deriving a closed form expression for Equation (24). According to [29], the expectation in Equation (24) can be written as a product of a modal rotation matrix $\hat{\mathbf{R}}$ and a symmetric matrix $\mathbf{S}$, depending on the concentration matrix $\mathbf{A}$:

$$\mathbb{E}(\mathbf{R}) = \hat{\mathbf{R}}^T\mathbf{S}. \tag{33}$$

Again, as in Equation (5), $\hat{\mathbf{R}}$ and $\mathbf{I} - \mathbf{S}$ are analogous to the circular mean and variance in the $\mathcal{SO}(2)$ case. The relationship between $\mathbf{S}$ and $\mathbf{A}$ is captured by two matrix functions $\mathbf{S} = \zeta(\mathbf{A})$ and its inverse $\mathbf{A} = \zeta^{-1}(\mathbf{S})$, derived in Appendix C.

It is easily verified, and shown in [41], that if $\mathbf{A}$ is diagonal so is $\mathbf{S}$. For

$$\begin{aligned} &\mathbf{A} = \mathrm{diag}(\kappa_1, \kappa_2, \kappa_3), \text{ where } \kappa_1 \geq \kappa_2 \geq |\kappa_3| > 0, \text{ and} \\ &\mathbf{S} = \mathrm{diag}(s_1, s_2, s_3), \text{ where } s_1 \geq s_2 \geq s_3, \end{aligned} \tag{34}$$

using just the first term in the asymptotic series of Equations (98) and (107) the matrix functions, $\mathbf{S} = \zeta(\mathbf{A})$ and its inverse $\mathbf{A} = \zeta^{-1}(\mathbf{S})$ are approximated by

$$\zeta(\mathbf{A}) \approx \mathrm{diag}\begin{pmatrix} 1 - \frac{1}{2\,(k_1+k_3)} - \frac{1}{2\,(k_1+k_2)} \\ 1 - \frac{1}{2\,(k_2+k_3)} - \frac{1}{2\,(k_1+k_2)} \\ 1 - \frac{1}{2\,(k_2+k_3)} - \frac{1}{2\,(k_1+k_3)} \end{pmatrix}, \tag{35}$$

and

$$\begin{aligned} &\zeta^{-1}(\mathbf{S}) \approx \frac{1}{2} \\ &\times [(s_3 + s_2 - s_1 - 1)(s_1 + s_2 - s_3 - 1)(s_1 + s_3 - s_2 - 1)]^{-1} \times \\ &\mathrm{diag}\begin{pmatrix} (-s_1 + s_2 + s_3 + 1)^2 + 2\,{s_1}^2 - 2\,{s_2}^2 - 2\,{s_3}^2 - 2 \\ (s_1 - s_2 + s_3 + 1)^2 - 2\,{s_1}^2 + 2\,{s_2}^2 - 2\,{s_3}^2 - 2 \\ (s_1 + s_2 - s_3 + 1)^2 - 2\,{s_1}^2 - 2\,{s_2}^2 + 2\,{s_3}^2 - 2 \end{pmatrix}. \end{aligned} \tag{36}$$

Using higher order terms of Equation (87) and (107), we could, in principle compute both ζ and ζ^{-1} to any desired accuracy. Notice, that ζ^{-1} in Equation (36) denotes a function inverse, not a matrix inverse.

For a non-diagonal concentration matrix $\mathbf{A} = \mathbf{V}\Sigma\mathbf{V}^T$, where V and Σ are the unitary matrix of eigenvectors and the diagonal matrix on eigenvalues, respectively, we write

$$\begin{aligned} \mathbb{E}(\mathbf{R}) &= \Lambda(\mathbf{A})\mathbf{V} \\ &\times \int_{\mathcal{SO}(3)} (\mathbf{V}^T\mathbf{R}) \exp\{\mathrm{Tr}[\hat{\mathbf{R}}^T\mathbf{V}\Sigma(\mathbf{V}^T\mathbf{R})]\}\, \mathrm{d}\nu(\mathbf{V}^T\mathbf{R}) \\ &= \hat{\mathbf{R}}^T\mathbf{V}\zeta(\Sigma)\mathbf{V}^T = \hat{\mathbf{R}}^T\zeta(\mathbf{A}). \end{aligned} \tag{37}$$

This yields

$$\zeta(\mathbf{A}) = \zeta(\mathbf{V}\Sigma\mathbf{V}^T) = \mathbf{V}\zeta(\Sigma)\mathbf{V}^T. \tag{38}$$

Similarly, we have

$$\zeta^{-1}[\zeta(\mathbf{A})] = \zeta^{-1}[\mathbf{V}\zeta(\Sigma)\mathbf{V}^T] = \mathbf{V}\zeta^{-1}[\zeta(\Sigma)]\mathbf{V}^T. \tag{39}$$

To summarise, to find the von Mises-Fisher distribution approximating the distribution of a random rotation matrix $\mathbf{R}$ with expectation $\mathbf{Z}$, we first compute the polar decomposition of $\mathbf{Z} = \hat{\mathbf{R}}^T\mathbf{S}$ and then choose $\hat{\mathbf{R}}$ and $\mathbf{A} = \zeta^{-1}(\mathbf{S})$ to be the rotational modal and concentration matrices for the von Mises-Fisher distribution, $\mathcal{VMF}(\mathbf{R}|\hat{\mathbf{R}}^T\mathbf{A})$.

A. Algorithm

We now describe the tracking algorithm.

a) Directional measurements and filter initialization: While many different measurement models can be incorporated under the general scheme proposed here, to be specific we assume N directional measurements, given as N three dimensional unit vectors in a local coordinate system. The measurements are acquired with errors from independent von Mises distributions on the sphere [26] with concentration parameters $\kappa_1, \ldots, \kappa_N$. We assume the local coordinate system rotates in space in some manner and that the directional measurements are collected at time instances t_k for $k = 0, \ldots, T-1$. The measurements are stacked into $3 \times N$ matrices $\mathbf{Y}_k = \mathbf{Y}(t_k)$ and, correspondingly, we define a concentration matrix $\mathbf{K} = \mathrm{diag}(\kappa_1, \ldots, \kappa_N)$. The aim of the tracker is to estimate the rotation of the local system at these time instances using the measurements $\mathbf{Y}_0, \ldots \mathbf{Y}_K$. The likelihood function for a given measurements $\mathbf{Y}_k$ (see [41] for details) is

$$\mathcal{L}(\mathbf{Y}_k|\mathbf{R}_k) = \Lambda(\mathbf{X}\mathbf{K}\mathbf{Y}_k^T) \exp[\mathrm{Tr}(\mathbf{X}\mathbf{K}\mathbf{Y}_k^T\mathbf{R}_k)]. \tag{40}$$

At $k = 0$ the $\mathcal{SO}(3)$ filter is initialized with a maximum likelihood estimate of $\mathbf{R}_{0|0}$ and $\mathbf{A}_{0|0}$ from initial directional measurements $\mathbf{Y}_0$

$$\mathbf{R}_{0|0}^T\mathbf{A}_{0|0} = \mathbf{X}\mathbf{K}\mathbf{Y}_0, \tag{41}$$

using Equation (32).

b) Prediction: In accordance with the Bayesian recursive filtering framework, we define a dynamical model which, at each discrete time instance, generates a distribution of a new unobserved rotation. In this section we consider two different cases for the dynamical model for the tracker, the first given by a random rotation and the second by a random angular velocity.

Generically the recursion starts with the posterior distribution at time $k-1$, which is

$$\mathrm{f}(\mathbf{R}_{k-1}|\mathbf{Y}_{k-1},\ldots,\mathbf{Y}_1) = \mathcal{VMF}(\mathbf{R}_{k-1}|\mathbf{R}_{k-1|k-1}^T\mathbf{A}_{k-1|k-1}). \tag{42}$$

for $k=1,\ldots,T$. The system dynamic model provides the prediction probability via the ChapmanKolmogorov equation, as described below.

1) Dynamics given by random rotation: As in the case of $\mathcal{SO}(2)$, random rotation dynamics assumes that , at time t_k, the orientation changes by another random rotation $\mathbf{P}$ with a von Mises-Fisher matrix distribution $\mathcal{VMF}(\mathbf{P}|\hat{\mathbf{P}}^T\mathbf{B})$. Thus the predicted orientation at time k is the product of two random rotations

$$\mathbf{Q}_k = \mathbf{P}\mathbf{R}_{k-1}. \tag{43}$$

To enable recursion we want to find a von Mises-Fisher matrix distribution that approximates the distribution of $\mathbf{Q}_k$ and, to this end, we write

$$\begin{aligned}\mathrm{f}(\mathbf{Q}_k) &= \Lambda(\mathbf{B})\Lambda(\mathbf{A}_{k-1|k-1}) \\ &\times \int_{\mathcal{SO}(3)} \exp[\mathrm{Tr}(\mathbf{R}_{k-1|k-1}^T\mathbf{A}_{k-1|k-1}\mathbf{R}_{k-1})] \\ &\times \exp[\mathrm{Tr}(\hat{\mathbf{P}}^T\mathbf{B}\mathbf{Q}_k\mathbf{R}_{k-1}^T)]\,\mathrm{d}\nu(\mathbf{R}_{k-1}).\end{aligned} \tag{44}$$

The expectation of $\mathbf{Q}_k$ with respect to this distribution is

$$\begin{aligned}\mathbb{E}_f(\mathbf{Q}_k) &= \Lambda(\mathbf{B})\Lambda(\mathbf{A}_{k-1|k-1}) \\ &\times \int_{\mathcal{SO}(3)} \mathbf{Q}_k \int_{\mathcal{SO}(3)} \exp[\mathrm{Tr}(\mathbf{R}_{k-1|k-1}^T\mathbf{A}_{k-1|k-1}\mathbf{R}_{k-1})] \\ &\times \exp[\mathrm{Tr}(\hat{\mathbf{P}}^T\mathbf{B}\mathbf{Q}_k\mathbf{R}_{k-1}^T)]\,\mathrm{d}\nu(\mathbf{R}_{k-1})\,\mathrm{d}\nu(\mathbf{Q}_k).\end{aligned} \tag{45}$$

After changing the order of integration and using the trace invariance under cyclic permutation we obtain

$$\begin{aligned}\mathbb{E}_f(\mathbf{Q}_k) &= \Lambda(\mathbf{B})\Lambda(\mathbf{A}_{k-1|k-1}) \\ &\times \int_{\mathcal{SO}(3)} \mathbf{Q}_k \int_{\mathcal{SO}(3)} \exp[\mathrm{Tr}(\mathbf{R}_{k-1|k-1}^T\mathbf{A}_{k-1|k-1}\mathbf{R}_{k-1})] \\ &\times \exp[\mathrm{Tr}(\hat{\mathbf{P}}^T\mathbf{B}\mathbf{Q}_k\mathbf{R}_{k-1}^T)]\,\mathrm{d}\nu(\mathbf{R}_{k-1})\,\mathrm{d}\nu(\mathbf{Q}_k).\end{aligned} \tag{46}$$

The inside integral, shown in curly brackets, is

$$\frac{1}{\Lambda(\mathbf{B}_k)}\zeta(\mathbf{B})\hat{\mathbf{P}}\mathbf{R}_{k-1}, \tag{47}$$

by Equation (37). In consequence, we have

$$\begin{aligned}&\mathbb{E}_f(\mathbf{Q}_k) = \Lambda(\mathbf{A}_{k-1|k-1})\zeta(\mathbf{B})\hat{\mathbf{P}} \\ &\times \int_{\mathcal{SO}(3)} \mathbf{R}_{k-1}\exp[\mathrm{Tr}(\mathbf{R}_{k-1|k-1}^T\mathbf{A}_{k-1|k-1}\mathbf{R}_{k-1})]\,\mathrm{d}\nu(\mathbf{R}_{k-1}).\end{aligned} \tag{48}$$

Applying Equation (37) again we arrive at

$$\mathbb{E}_f(\mathbf{Q}_k) = \zeta(\mathbf{B})\hat{\mathbf{P}}\zeta(\mathbf{A}_{k-1|k-1})\mathbf{R}_{k-1|k-1}. \tag{49}$$

Finally, the predicted modal and concentration matrices $\mathbf{R}_{k|k-1}$ and $\mathbf{A}_{k|k-1}$ are computed from $\mathbb{E}_f(\mathbf{Q}_k)$ via the algorithm outlined in III-0a.

It is interesting to notice that, while Equation (49), entails that $\mathbb{E}_f(\mathbf{Q}_k)$ is equal to the product of $\mathbb{E}(\mathbf{P})$ and $\mathbb{E}(\mathbf{R}_{k-1})$, unlike in the $\mathcal{SO}(2)$ case in Equation (15), the modal rotation of $\mathbf{Q}_k$ is not equal to the product of the modal rotations $\hat{\mathbf{P}}$ and $\mathbf{R}_{k-1}$, because of non-commutativity.

2) Dynamics given by Random Angular Velocity: In many practical applications the dynamics is better modelled by a random vector of angular velocity, specified by a random tangent vector $\boldsymbol{w}'$. The prediction step in this case is different. The angular velocity vector $\boldsymbol{w}' \in \mathbb{R}^3$, the tangent space of $\mathcal{SO}(3)$, and a choice of a tri-variate normal distribution $\mathcal{N}(\boldsymbol{w}'|\boldsymbol{w}_0', \Psi')$ with mean $\boldsymbol{w}_0'$ and covariance Ψ' for it is more appropriate. Now, define

$$\begin{aligned}\boldsymbol{w} &= \boldsymbol{w}'\Delta t, \\ \boldsymbol{w}_0 &= \boldsymbol{w}_0'\Delta t, \\ \Psi &= \Psi'\Delta t^2,\end{aligned} \tag{50}$$

where Δt is time between epochs. As for the $\mathcal{SO}(2)$ case in Equation (9), we find the relationship between the von Mises-Fisher distribution on $\mathcal{SO}(3)$ and the Gaussian on its tangent space at $\boldsymbol{w}_0$ by computing Taylor expansion of

$$\mathrm{Tr}(\mathbf{B}\mathbf{R}_{\boldsymbol{w}_0}^T\mathbf{R}_{\boldsymbol{w}}), \tag{51}$$

described in Appendix D, and then proceed as in Section III-A1. Equating the second order terms in the exponents of $\mathcal{N}(\boldsymbol{w}|\boldsymbol{w}_0,\Psi)$ and $\mathcal{VMF}(\mathbf{P}|\mathbf{R}_{\boldsymbol{w}_0}^T\mathbf{B})$ yields

$$\mathbf{G}_{\boldsymbol{w}_0}^T\tilde{\mathbf{B}}\mathbf{G}_{\boldsymbol{w}_0} = -\Psi^{-1}, \tag{52}$$

where $\mathbf{G}_{\boldsymbol{w}_0}$ is defined in Equation (83). It follows that

$$\tilde{\mathbf{B}} = -\mathbf{G}_{\boldsymbol{w}_0}^{-T}\Psi^{-1}\mathbf{G}_{\boldsymbol{w}_0}^{-1}, \tag{53}$$

The matrix $\mathbf{B}$ is then recovered by

$$\mathbf{B} = -\frac{1}{2}\mathrm{Tr}(\tilde{\mathbf{B}})\mathbf{I} + \tilde{\mathbf{B}}. \tag{54}$$

The distribution of the dynamics is given by $\mathcal{VMF}(\mathbf{P}|\mathbf{R}_{\boldsymbol{w}_0}^T\mathbf{B})$ in terms of $\boldsymbol{w}_0$ and Ψ. This approximation, as in the $\mathcal{SO}(2)$ filter, relies on Ψ being small.

Finally the predicted modal and concentration matrices, $\mathbf{R}_{k|k-1}$ and $\mathbf{A}_{k|k-1}$ are computed via Equation (49) and the algorithm in III-0a.

a) Bayesian update: Bayes' Rule gives the posterior distribution

$$\begin{aligned}\mathrm{f}(\mathbf{R}_k|\mathbf{Y}_k,\ldots,\mathbf{Y}_1) &\propto \mathcal{L}(\mathbf{Y}_k|\mathbf{Q}_k)\,\mathrm{f}(\mathbf{Q}_k) = \\ &\exp[\mathrm{Tr}(\mathbf{X}\mathbf{K}\mathbf{Y}_k^T\mathbf{R}_k + \mathbf{R}_{k|k-1}^T\mathbf{A}_{k|k-1}\mathbf{R}_k)],\end{aligned} \tag{55}$$

where $\mathcal{L}(\mathbf{Y}_k|\mathbf{Q}_k)$ is given in Equation (40). To complete the update we need to compute the modal and concentration matrices $\mathbf{R}_{k|k}$ and $\mathbf{A}_{k|k}$ of Equation (55) using the polar decomposition in Equation (32) applied to

$$\mathbf{C} = \mathbf{X}\mathbf{K}\mathbf{Y}_k^T + \mathbf{R}_{k|k-1}^T\mathbf{A}_{k|k-1}. \tag{56}$$

The final expression for the posterior distribution is

$$\mathrm{f}(\mathbf{R}_k|\mathbf{Y}_k,\ldots,\mathbf{Y}_1) = \mathcal{VMF}(\mathbf{R}_k|\mathbf{R}_{k|k}^T\mathbf{A}_{k|k}). \tag{57}$$

This completes the recursion of the $\mathcal{SO}(3)$ filter. In a similar way to all other recursive filters, the prediction and update

phases alternate, with the prediction progressing the state until the next measurement is available, and the update assimilating the measurement.

A complete algorithm for recursive estimation in $\mathcal{SO}(3)$ filter is provided by Equations (49), (55) and (57).

B. Numerical results

Tracking on $\mathcal{SO}(3)$ occurs in a wide range of applications, associated with rotations of a rigid body in an inertial frame, for example tracking the attitude and stabilization of flying drones and floating buoys, tracking of human and animal body movement (where multiple connected rigid bodies are modelled), tracking of the trajectory of a vehicle in combination with GPS measurements, etc.

Here we illustrate the ideas presented in Section III with measurements from a simulated IMU. The sensors in a typical IMU are a 3-axes accelerometer, a 3-axes gyroscope and a 3-axes magnetometer. The magnetometer and the accelerometer both provide noisy directional measurements in the direction to the Earth's North Pole, and the direction of the Earth's gravitational acceleration respectively, at that point on the Earth's surface.

The gyroscope provides noisy measurements of angular velocity, which we insert into the tracker in the prediction stage. Here, we represent the dynamic at the k'th epoch by a Gaussian with mean $\boldsymbol{w}_k$ (the actual gyroscope measurement) and covariance $\Psi = \sigma_w^2 \mathbf{I}$, where σ_w is specified by the gyroscope standard error.

The aim of these experiments is to track the self-orientation of the IMU. The measurements are processed, for comparison, with the $\mathcal{SO}(3)$ filter and with

- the Extended Kalman Filter (EKF), implemented to track the Euler angles of the orientation;
- the Complementary Filter of Mahony *et al.* [24].

The EKF tracker uses a linear approximation to the state space $\mathcal{SO}(3)$ and to the dynamical model but, because the addition of Gaussian noise (in the tangent space) to a rotation matrix does not in general result in another rotation matrix, this method requires some way of "projecting" the state back into $\mathcal{SO}(3)$. Because of this lack of fidelity in the choice of the noise model, the EKF requires frequent re-initialization of the tracker, manifested by singularities in the posterior covariance. This results in often misleadingly small tracking errors.

The Complimentary Filter (CF), in effect a constant gain tracker, overcomes this "departure from the manifold" problem, but does not provide a mechanism for computing the error in the estimator. For these trackers only *ad hoc* internal methods for correction of the track are available, based on metrics to determine whether a "bad" measurement is received.

For the experiments, the IMU measurements are simulated at 100 Hz sampling rate while the IMU is performing rotations around each of the three axes in turn at constant speed. The measurement noise standard deviations are chosen to mimic IMU measurements from a typical iphone: that is, 0.01 G for each axis of the accelerometer, 0.1 rad for each gyroscope axis, and 0.4 μT for each magnetometer direction. Doing this in simulations provides a comparison of the results with the ground truth. This is typically not easily available with real data. A subsequent paper will be concerned with details about an IMU-specific tracker and applications to real data.

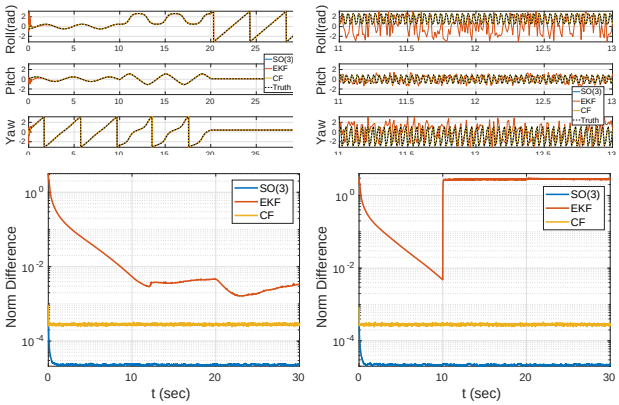

Fig. 2. Results of Experiments 1 and 2. Top panels: Example of tracking in terms of Euler angles with $\mathcal{SO}(3)$, EKF and complementary filters for rotation at slow (left panel) and a 2 sec fragment of fast (right panel) rates. While the $\mathcal{SO}(3)$ filter follows the tracks exactly, the EKF struggle to keep up even at slow rate. In fast rate it fails to recover the correct orientation when the direction of rotation changed. CF's performance is acceptable and similar in both the slow and the fast experiments. Bottom panels: averaged over 1000 MC runs $L_F(t)$ for each of the three filters; left panel shows results for the experiments at slow, right panel at fast rotational speeds. Both panels show similar values for $SO(3)$ tracker, which out-perform EKF and CF in both cases.

The first two experiments involve 1000 Monte-Carlo simulations of a 30 second collection of data during which the IMU is exercising constant speed rotations of 10 seconds about each of the x-axis, y-axis, and z-axis in turn. The initial orientation of an IMU is selected randomly. In the first experiment the rotation speed is set to 0.5π radians per second (slow) and in the second the rotation speed is 50π radians per second (fast). Plots depicting the resulting estimated Euler angles along with the ground truth are shown in Figure 2; the left panel for slow experiment, and the right for the fast experiment. In addition, we evaluated the distance in the $\mathcal{SO}(3)$ group between the estimated and true values, using the Frobenius norm as the performance metric. This is

$$L_F(t) = 3 - \mathrm{Tr}[\hat{\mathbf{R}}(t)\mathbf{R}^T(t)], \tag{58}$$

where $\hat{\mathbf{R}}(t)$ is the estimate of the orientation at time t and $\mathbf{R}$ is the rotation matrix of the actual orientation (ground truth). The resulting average across runs $L_F(t)$ is presented in the bottom panels of Figure 2

The third set of experiments involve rotation at random speeds around a random axis (not necessarily around the x, y or z axes) at each time sample. The directions of the rotation and the rotational speeds are given in terms of an angular velocity vector as a 3-variate Gaussian with mean zero and covariance $(6\pi)^2 I$ (rad/sec)^2, where I is a 3×3 identity matrix. Again the sampling is at 100Hz over a period of 30 seconds. A total of 1000 Monte Carlo runs are performed. The results are presented in Figure 3. The top panel shows an example of such random rotations and their reconstruction using the $SO(3)$ filter, the EKF and the CF. The bottom left panel shows a magnified small section of the plot in the top

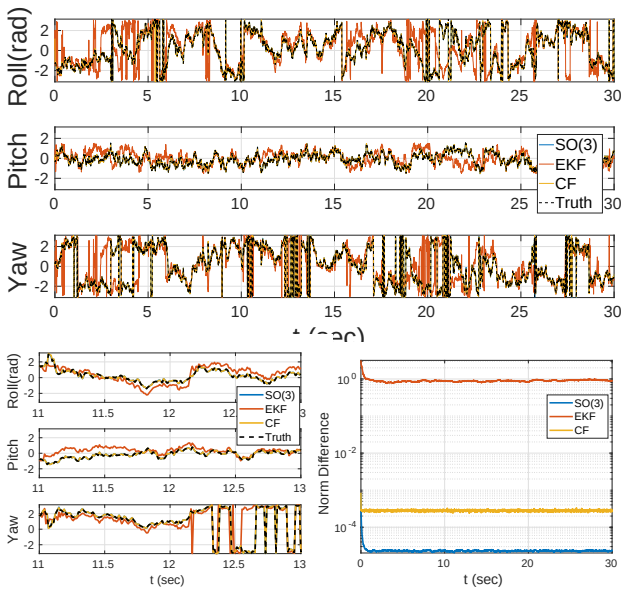

Fig. 3. The top panel shows an example of a random rotation in terms of Euler angles and its reconstructions for $SO(3)$ filter, EKF and CF. The bottom left panel shows a 2 sec fragment of the plot on the top panel; the bottom right is averaged over 1000 MC runs $L_F(t)$ for each of the three filters.

panel, while the bottom right shows the average $L_F(t)$ for each of the three filters. It follows from comparison of average errors in Figures 2 and 3 that the performance of $\mathcal{SO}(3)$ and CF filters is not sensitive to the manner of rotation, while the performance for the EKF strongly depends on it. The $SO(3)$ filter clearly outperforms both of the other two filters each time in all three experiments.

IV. Conclusion

We have described a tracking algorithm based on Bayesian recursion to perform tracking on the rotation groups $\mathcal{SO}(2)$ and $\mathcal{SO}(3)$ with applications to rigid body motion in $\mathbf{R}^2$ and $\mathbf{R}^3$. While tracking in $\mathcal{SO}(2)$, based on the (maximal entropy) von Mises distribution, is relatively straightforward and only requires computation of a one dimensional variable, tracking on $\mathcal{SO}(3)$ is complicated by the fact that three dimensional rotations do not commute and calculations in the Lie algebra have to be used.

The tracker can encompass a range of measurement models and is specifically designed to track the orientation in three dimensions with, for instance, directional measurements. Where approximations are forced to enable recursion, the maximum entropy distribution with the same location and spread parameters are used to ensure no unwarranted assumptions about estimation errors are made. By comparison, trackers such as the EKF tend to make such assumptions, resulting in estimates of the state errors that are significantly smaller than actual errors and hence loss of track.

The state distributions used in this tracker are appropriate to the context and result in an elegant, fast, and accurate algorithm that does not require re-initialization at any time and gives a realistic estimate of the statistical errors of the underlying parameters. We show in simulations that the tracking algorithm outperforms both the EKF and the Complementary Filter when compared using simulated data.

A subsequent paper will focus on applications and will, in particular, include an $\mathcal{SO}(3)$ tracking pseudo-code, specific to the IMU measurements and experimental results with real IMU data.

References

[1] P. D. Groves, *Principles of GNSS, inertial, and multisensor integrated navigation systems*. 2013.

[2] N. Sugimura, K. Fukuda, Y. Tomioka, M. Fukuyama, Y. Sakamoto, T. Kuwahara, T. Fukuhara, K. Yoshida, and Y. Takahashi, "Ground test of attitude control system for micro satellite rising-2," in *System Integration (SII), 2012 IEEE/SICE International Symposium on*, pp. 301–306, IEEE, 2012.

[3] R. Kristiansen, P. J. Nicklasson, and J. T. Gravdahl, "Satellite attitude control by quaternion-based backstepping," *Control Systems Technology, IEEE Transactions on*, vol. 17, no. 1, pp. 227–232, 2009.

[4] K. Izumida and R. Kasai, "Artificial satellite attitude control system," Oct. 14 1986. US Patent 4,617,634.

[5] L. Muhlfelder, J. E. Keigler, and B. Stewart, "Momentum biased active three-axis satellite attitude control system," Jan. 31 1978. US Patent 4,071,211.

[6] P. Khosla and T. Kanade, "Real-time implementation and evaluation of model-based controls on cmu dd arm ii," in *Robotics and Automation. Proceedings. 1986 IEEE International Conference on*, vol. 3, pp. 1546–1555, IEEE, 1986.

[7] B. Barshan and H. Durrant-Whyte, "Inertial navigation systems for mobile robots," *Robotics and Automation, IEEE Transactions on*, vol. 11, no. 3, pp. 328–342, 1995.

[8] A. M. Walker, D. P. Miller, and C. Ling, "Spatial orientation aware smartphones for tele-operated robot control in military environments a usability experiment," in *Proceedings of the Human Factors and Ergonomics Society Annual Meeting*, vol. 57, pp. 2027–2031, SAGE Publications, 2013.

[9] C.-H. Zheng, "A study of hybrid position/impedance control applied to peg-in-hole task with robot arm," 2013.

[10] S. Ozel, S. E. Eskimez, and K. Erbatur, "Humanoid robot orientation stabilization by shoulder joint motion during locomotion," in *Control Conference (ASCC), 2013 9th Asian*, pp. 1–6, IEEE, 2013.

[11] E. Bachmann, I. Duman, U. Usta, R. McGhee, X. Yun, and M. Zyda, "Orientation tracking for humans and robots using inertial sensors," in *Computational Intelligence in Robotics and Automation, 1999. CIRA'99. Proceedings. 1999 IEEE International Symposium on*, pp. 187–194, IEEE, 1999.

[12] M. Šenk and L. Chèze, "Rotation sequence as an important factor in shoulder kinematics," *Clinical biomechanics*, vol. 21, pp. S3–S8, 2006.

[13] J. Calusdian, "A personal navigation system based on inertial and magnetic field measurements," 2010.

[14] L. Bai, M. Pepper, Y. Yan, S. Spurgeon, M. Sakel, and M. Phillips, "A multi-parameter assessment tool for upper limb motion in neurorehabilitation," in *Instrumentation and Measurement Technology Conference (I2MTC), 2011 IEEE*, pp. 1–4, IEEE, 2011.

[15] M. El-Gohary, L. Holmstrom, J. Huisinga, E. King, J. McNames, and F. Horak, "Upper limb joint angle tracking with inertial sensors," in *Engineering in Medicine and Biology Society, EMBC, 2011 Annual International Conference of the IEEE*, pp. 5629–5632, IEEE, 2011.

[16] A. Erol, G. Bebis, M. Nicolescu, R. Boyle, and X. Twombly, "Vision-based hand pose estimation: A review," *Computer Vision and Image Understanding*, vol. 108, no. 1, pp. 52–73, 2007.

[17] E. Lefferts, F. Markley, and M. Shuster, "Kalman filtering for spacecraft attitude estimation," *Journal of Guidance, Control, and Dynamics*, vol. 5, no. 5, pp. 417–429, 1982.

[18] S. Stančin and S. Tomažič, "Angle estimation of simultaneous orthogonal rotations from 3D gyroscope measurements," *Sensors*, vol. 11, no. 9, pp. 8536–8549, 2011.

[19] A. Sabatini, "Quaternion-based extended Kalman filter for determining orientation by inertial and magnetic sensing," *Biomedical Engineering, IEEE Transactions on*, vol. 53, no. 7, pp. 1346–1356, 2006.

[20] R. Zhu, D. Sun, Z. Zhou, and D. Wang, "A linear fusion algorithm for attitude determination using low cost MEMS-based sensors," *Measurement*, vol. 40, no. 3, pp. 322–328, 2007.

[21] N. Phuong, H. Kang, Y. Suh, and Y. Ro, "A DCM based orientation estimation algorithm with an inertial measurement unit and a magnetic compass," *Journal of Universal Computer Science*, vol. 15, no. 4, pp. 859–876, 2009.

[22] R. Mahony, T. Hamel, and J. Pflimlin, "Complementary filter design on the special orthogonal group $\mathcal{SO}(3)$," in *Decision and Control, 2005 and 2005 European Control Conference. CDC-ECC'05. 44th IEEE Conference on*, pp. 1477–1484, IEEE, 2005.

[23] T. Hamel and R. Mahony, "Attitude estimation on $\mathcal{SO}(3)$ based on direct inertial measurements," in *Robotics and Automation, 2006. ICRA 2006. Proceedings 2006 IEEE International Conference on*, pp. 2170–2175, IEEE, 2006.

[24] R. Mahony, T. Hamel, and J. Pflimlin, "Nonlinear complementary filters on the special orthogonal group," *Automatic Control, IEEE Transactions on*, vol. 53, no. 5, pp. 1203–1218, 2008.

[25] T. Downs, "Orientation statistics," *Biometrika*, vol. 59, no. 3, pp. 665–676, 1972.

[26] A. James, "Distributions of matrix variates and latent roots derived from normal samples," *The Annals of Mathematical Statistics*, pp. 475–501, 1964.

[27] A. James, "Normal multivariate analysis and the orthogonal group," *The Annals of Mathematical Statistics*, pp. 40–75, 1954.

[28] P. Jupp and K. Mardia, "Maximum likelihood estimators for the matrix von Mises-Fisher and Bingham distributions," *The Annals of Statistics*, vol. 7, no. 3, pp. 599–606, 1979.

[29] C. Khatri and K. Mardia, "The von Mises-Fisher matrix distribution in orientation statistics," *Journal of the Royal Statistical Society. Series B (Methodological)*, pp. 95–106, 1977.

[30] E. Hewitt and K. A. Ross, *Abstract Harmonic Analysis: Volume I Structure of Topological Groups Integration Theory Group Representations*, vol. 115. Springer Science & Business Media, 2012.

[31] A. James, "Zonal polynomials of the real positive definite symmetric matrices," *The Annals of Mathematics*, vol. 74, no. 3, pp. 456–469, 1961.

[32] M. Moakher, "Means and averaging in the group of rotations," *SIAM Journal on Matrix Analysis and Applications*, vol. 24, no. 1, pp. 1–16, 2002.

[33] L. Imlahi and A. Chakak, "A study of the tangent space model of the von Mises-Fisher distribution," *Revista de la Real Academia de Ciencias Exactas, Físicas y Naturales. Serie A: Matemáticas (RACSAM)*, vol. 97, no. 1, pp. 41–52, 2003.

[34] P. Kim, "On the characteristic function of the von Mises-Fisher matrix distribution," in *High Dimensional Probability II* (D. M. E. Gine and J. Wellner, eds.), (Boston), pp. 477–492, Birkhäuser, 2000.

[35] G. Watson, "Distributions on the circle and sphere," *Journal of Applied Probability*, pp. 265–280, 1982.

[36] G. Kurz, I. Gilitschenski, and U. D. Hanebeck, "Recursive bayesian filtering in circular state spaces," *IEEE Aerospace and Electronic Systems Magazine*, vol. 31, no. 3, pp. 70–87, 2016.

[37] G. Kurz, I. Gilitschenski, and U. D. Hanebeck, "Unscented von mises–fisher filtering," *IEEE Signal Processing Letters*, vol. 23, no. 4, pp. 463–467, 2016.

[38] F. Chatelain and N. Le Bihan, "von mises-fisher approximation of multiple scattering process on the hypersphere," in *Acoustics, Speech and Signal Processing (ICASSP), 2013 IEEE International Conference on*, pp. 6461–6465, IEEE, 2013.

[39] K. Mardia and P. Jupp, *Directional Statistics*, vol. 28. Wiley, 2000.

[40] A. Laforgia and P. Natalini, "Some inequalities for modified bessel functions," *Journal of Inequalities and Applications*, vol. 2010, no. 1, p. 253035, 2010.

[41] I. Clarkson, S. Howard, W. Moran, D. Cochran, and M. Dawson, "Maximum-likelihood and best invariant orientation estimation," in *Signals, Systems and Computers (ASILOMAR), 2010 Conference Record of the Forty Fourth Asilomar Conference on*, pp. 1996–2000, IEEE, 2010.

[42] R. M. Wilcox, "Exponential operators and parameter differentiation in quantum physics," *Journal of Mathematical Physics*, vol. 8, no. 4, pp. 962–982, 1967.

APPENDIX A. ANGLE-AXIS REPRESENTATION OF ELEMENTS OF $\mathcal{SO}(3)$

An element of $\mathcal{SO}(3)$ can be written uniquely in the form

$$\mathbf{R}_{\boldsymbol{w}} = \exp[\boldsymbol{L}(\boldsymbol{w})], \tag{59}$$

with

$$\|\boldsymbol{L}(\boldsymbol{w})\|_E = \sqrt{\mathrm{Tr}\left(\boldsymbol{L}(\boldsymbol{w})\boldsymbol{L}(\boldsymbol{w})^{\mathsf{T}}\right)} < \sqrt{2\pi}, \tag{60}$$

where $\boldsymbol{w} = (w_1, w_2, w_3) \in \mathbb{R}^3$ and $\boldsymbol{L}(\boldsymbol{w})$ is the real anti-symmetric matrix

$$\boldsymbol{L}(\boldsymbol{w}) = \sum_{j=1}^{3} w_j L_j. \tag{61}$$

Here

$$L_1 = \begin{pmatrix} 0 & 0 & 0 \\ 0 & 0 & 1 \\ 0 & -1 & 0 \end{pmatrix}, \; L_2 = \begin{pmatrix} 0 & 0 & -1 \\ 0 & 0 & 0 \\ 1 & 0 & 0 \end{pmatrix}, \; L_3 = \begin{pmatrix} 0 & 1 & 0 \\ -1 & 0 & 0 \\ 0 & 0 & 0 \end{pmatrix} \tag{62}$$

is a basis for the 3×3 skew-symmetric matrices. Such matrices naturally constitute the tangent space of $\mathcal{SO}(3)$ at the identity (the Lie algebra of $\mathcal{SO}(3)$). The subscript of $\mathbf{R}_{\boldsymbol{w}}$, which associates the rotation matrix with its angle-axis parametrization [29], is omitted when unnecessary. The characteristic equation for $\boldsymbol{L}(\boldsymbol{w})$ is

$$\lambda^3 = -\|\boldsymbol{w}\|^2\lambda, \tag{63}$$

and so the eigenvalues of $\boldsymbol{L}(\boldsymbol{w})$ are $\{i\|\boldsymbol{w}\|, -i\|\boldsymbol{w}\|, 0\}$. The CayleyHamilton theorem yields

$$\boldsymbol{L}(\boldsymbol{w})^3 = -\|\boldsymbol{w}\|^2\boldsymbol{L}(\boldsymbol{w}). \tag{64}$$

Expanding $\mathbf{R}_{\boldsymbol{w}}$ we have *Rodrigues' rotation formula*

$$\begin{aligned} \mathbf{R}_{\boldsymbol{w}} &= \mathbf{I} + \sum_{n=1}^{\infty} \frac{1}{n!}\boldsymbol{L}(\boldsymbol{w})^n \\ &= \mathbf{I} + \sin\|\boldsymbol{w}\|\boldsymbol{L}(\hat{\boldsymbol{w}}) + (1 - \cos\|\boldsymbol{w}\|)\boldsymbol{L}(\hat{\boldsymbol{w}})^2, \end{aligned} \tag{65}$$

where $\hat{\boldsymbol{w}} = \frac{\boldsymbol{w}}{\|\boldsymbol{w}\|}$. To compute Haar measure in this parameterization we consider the invariant $\mathbf{R}_{\boldsymbol{w}}^T \, \mathrm{d}\mathbf{R}_{\boldsymbol{w}}$. For any $\boldsymbol{w}, \mathbf{a} \in \mathbb{R}^3$, we have

$$\mathbf{R}_{\boldsymbol{w}}\boldsymbol{L}(\mathbf{a})\mathbf{R}_{\boldsymbol{w}}^{-1} = e^{\boldsymbol{L}(\boldsymbol{w})}\boldsymbol{L}(\mathbf{a})e^{-\boldsymbol{L}(\boldsymbol{w})} = \boldsymbol{L}(\mathbf{R}_{\boldsymbol{w}}\mathbf{a}). \tag{66}$$

Using Equation (2.1) of [42], we obtain

$$\mathrm{d}\mathbf{R}_{\boldsymbol{w}} = \int_0^1 e^{(1-t)\boldsymbol{L}(\boldsymbol{w})}\boldsymbol{L}(d\boldsymbol{w})e^{t\boldsymbol{L}(\boldsymbol{w})}dt, \tag{67}$$

and so

$$\mathbf{R}_{\boldsymbol{w}}^T \, \mathrm{d}\mathbf{R}_{\boldsymbol{w}} = \int_0^1 e^{-t\boldsymbol{L}(\boldsymbol{w})}\boldsymbol{L}(d\boldsymbol{w})e^{t\boldsymbol{L}(\boldsymbol{w})}dt. \tag{68}$$

Taking account of the property in Equation (66) yields

$$\mathbf{R}_{\boldsymbol{w}}^T \, \mathrm{d}\mathbf{R}_{\boldsymbol{w}} = \boldsymbol{L}(\mathbf{G}_{\boldsymbol{w}}d\boldsymbol{w}), \tag{69}$$

where $\mathbf{G}_{\boldsymbol{w}}$ is the matrix

$$\begin{aligned} \mathbf{G}_{\boldsymbol{w}} &= \int_0^1 e^{-t\boldsymbol{L}(\boldsymbol{w})}dt \\ &= \mathbf{I} + \frac{1 - \cos\|\boldsymbol{w}\|}{\|\boldsymbol{w}\|}\boldsymbol{L}(\hat{\boldsymbol{w}}) + \left(1 - \frac{\sin\|\boldsymbol{w}\|}{\|\boldsymbol{w}\|}\right)\boldsymbol{L}(\hat{\boldsymbol{w}})^2. \end{aligned} \tag{70}$$

Notice that

$$\lim_{\|\boldsymbol{w}\|=0} \mathbf{G}_{\boldsymbol{w}} = \mathbf{I}. \tag{71}$$

Haar measure is then, up to normalization,

$$\det \mathbf{G}_{\boldsymbol{w}} \prod_{j=1}^{3} dw_j. \tag{72}$$

To calculate $\det \mathbf{G}_{\boldsymbol{w}}$ note that $\mathbf{G}_{\boldsymbol{w}}$ has the same eigenvectors as $\boldsymbol{L}(\boldsymbol{w})$ and, if $\lambda \neq 0$ is an eigenvalue of $\boldsymbol{L}(\boldsymbol{w})$, then

$$\int_0^1 e^{-t\lambda} dt \tag{73}$$

is an eigenvalue of $\mathbf{G}_{\boldsymbol{w}}$. Thus, the eigenvalues of $\mathbf{G}_{\boldsymbol{w}}$ are

$$\left\{ \frac{1-e^{i\|\boldsymbol{w}\|}}{i\|\boldsymbol{w}\|}, \frac{1-e^{-i\|\boldsymbol{w}\|}}{-i\|\boldsymbol{w}\|}, 1 \right\}, \tag{74}$$

and consequently

$$\det \mathbf{G}_{\boldsymbol{w}} = \frac{2(1-\cos\|\boldsymbol{w}\|)}{\|\boldsymbol{w}\|^2}. \tag{75}$$

Normalized Haar measure is then

$$\mathrm{d}\nu(\mathbf{R}) = \frac{(1-\cos\|\boldsymbol{w}\|)}{4\pi^2\|\boldsymbol{w}\|^2} \prod_{j=1}^{3} dw_j. \tag{76}$$

Appendix B. Asymptotic expansion of $\Lambda(\mathbf{W})$

We compute here the approximate formula for

$$\Lambda(\Sigma) = \int_{\mathcal{SO}(3)} \exp \mathrm{Tr}(\Sigma\mathbf{R})\, \mathrm{d}\nu(\mathbf{R}), \tag{77}$$

where $\Sigma = \mathrm{diag}(\kappa_1, \kappa_2, \kappa_3)$ is the matrix of eigenvalues of $\mathbf{W}$ and $\mathrm{d}\nu(\mathbf{R})$ is normalized Haar measure on $\mathcal{SO}(3)$. Using Rodrigues' formula (Equation (65)) and writing

$$q(x) = \frac{1-\cos x}{x^2}, \tag{78}$$

we obtain

$$\Lambda(\Sigma) = \frac{1}{4\pi^2} e^{\mathrm{Tr}(\Sigma)} \int_{\|\boldsymbol{w}\|<\pi} q(\|\boldsymbol{w}\|) \exp\left[-\boldsymbol{w}^{\mathsf{T}} \tilde{\Sigma} \boldsymbol{w}\, q(\|\boldsymbol{w}\|) \right] d\boldsymbol{w}, \tag{79}$$

where

$$\tilde{\Sigma} = \begin{pmatrix} \kappa_2+\kappa_3 & 0 & 0 \\ 0 & \kappa_1+\kappa_3 & 0 \\ 0 & 0 & \kappa_1+\kappa_2 \end{pmatrix}. \tag{80}$$

Now we make the change of variable, $\boldsymbol{y} \leftrightarrow \boldsymbol{w}$

$$\boldsymbol{y} = \sqrt{q(\|\boldsymbol{w}\|)}\boldsymbol{w}, \qquad \boldsymbol{w} = s(\|\boldsymbol{y}\|)\boldsymbol{y}, \tag{81}$$

where s is the function

$$s(x) = \frac{\cos^{-1}(1-x^2)}{x}, \tag{82}$$

so that

$$q(||\boldsymbol{w}||) = \frac{1}{s(||\boldsymbol{y}||)^2}. \tag{83}$$

This change of variable has Jacobian

$$J = s(\|\boldsymbol{y}\|) I + \frac{s'(\|\boldsymbol{y}\|)}{\|\boldsymbol{y}\|} \boldsymbol{y}\boldsymbol{y}^{\mathsf{T}}, \tag{84}$$

so that the matrix determinant lemma yields

$$\begin{aligned} \det J &= \left[1 + \frac{s'(\|\boldsymbol{y}\|)}{s(\|\boldsymbol{y}\|)} \|\boldsymbol{y}\| \right] s(\|\boldsymbol{y}\|)^3 \\ &= s(\|\boldsymbol{y}\|)^2 \left[s(\|\boldsymbol{y}\|) + \|\boldsymbol{y}\| s'(\|\boldsymbol{y}\|) \right]. \end{aligned} \tag{85}$$

With Equation (83) this produces

$$\begin{aligned} &\Lambda(\Sigma) = \\ &= \frac{1}{4\pi^2} e^{\mathrm{Tr}(\tilde{\Sigma})/2} \int\limits_{\|\boldsymbol{y}\|^2<2} \left[s(\|\boldsymbol{y}\|) + \|\boldsymbol{y}\| s'(\|\boldsymbol{y}\|) \right] \exp\left(-\boldsymbol{y}^{\mathsf{T}} \tilde{\Sigma} \boldsymbol{y} \right) d\boldsymbol{y} \\ &= \frac{\sqrt{2}}{4\pi^2} e^{\mathrm{Tr}(\tilde{\Sigma})/2} \int\limits_{\|\boldsymbol{y}\|^2<2} \frac{1}{\sqrt{1-\|\boldsymbol{y}\|^2/2}} \exp\left(-\boldsymbol{y}^{\mathsf{T}} \tilde{\Sigma} \boldsymbol{y} \right) d\boldsymbol{y}. \end{aligned} \tag{86}$$

Using the Taylor expansion for the first term in the integrand we have

$$\Lambda(\Sigma) \sim \frac{1}{4}\sqrt{\frac{2}{\pi}} e^{\mathrm{Tr}(\tilde{\Sigma})/2} (\det \tilde{\Sigma})^{-1/2} \sum_{n=0}^{\infty} a_n M_{2n}\left(\tilde{\Sigma}\right), \tag{87}$$

where $a_n = (1, 1/4, 3/32, 5/128, 35/2048, 63/8192, \ldots)$ are the coefficients of the Taylor expansion of $1/\sqrt{1-x/2}$ and

$$M_{2n}(\tilde{\Sigma}) = \frac{(\det \tilde{\Sigma})^{1/2}}{(\pi)^{3/2}} \int_{\mathbb{R}^3} \|\boldsymbol{y}\|^{2n} \exp\left(-\boldsymbol{y}^{\mathsf{T}} \tilde{\Sigma} \boldsymbol{y} \right) d\boldsymbol{y}. \tag{88}$$

This change of limits of integration is appropriate for large values of κ_i, because the integrand is essentially contained in the ball $||\boldsymbol{y}||^2 < 2$.

Consider the moment generating function

$$\begin{aligned} \Phi(t) &= \frac{(\det \tilde{\Sigma})^{1/2}}{(\pi)^{3/2}} \int_{\mathbb{R}^3} \exp\left[-\boldsymbol{y}^{\mathsf{T}} (\tilde{\Sigma} + tI) \boldsymbol{y} \right] d\boldsymbol{y} \\ &= \det(t\tilde{\Sigma}^{-1} + I)^{-1/2} \\ &= \frac{1}{\sqrt{S_3 t^3 + S_2 t^2 + S_1 t + 1}}, \end{aligned} \tag{89}$$

where the S_i are the elementary symmetric polynomials of $\kappa_i = (\kappa_j + \kappa_k)^{-1}$ with i, j, k distinct ($i, j, k = 1, 2, 3$):

$$\begin{aligned} S_1 &= \mathrm{Tr}\left(\tilde{\Sigma}^{-1}\right) = \tilde{\kappa}_1 + \tilde{\kappa}_2 + \tilde{\kappa}_3, \\ S_2 &= \tilde{\kappa}_1\tilde{\kappa}_2 + \tilde{\kappa}_2\tilde{\kappa}_3 + \tilde{\kappa}_3\tilde{\kappa}_1, \\ S_3 &= \det\left(\tilde{\Sigma}^{-1}\right) = \tilde{\kappa}_1\tilde{\kappa}_2\tilde{\kappa}_3. \end{aligned} \tag{90}$$

Now $M_{2n}(\tilde{\Sigma}) = (-1)^n n!\, \Phi^{(n)}(0)$ and so

$$\begin{aligned} M_2(\tilde{\Sigma}) &= \frac{1}{2} S_1, \\ M_4(\tilde{\Sigma}) &= \frac{1}{4}\left(3S_1^2 - 4S_2\right), \\ M_6(\tilde{\Sigma}) &= \frac{3}{8}\left(5S_1^3 - 12S_1S_2 + 8S_3\right), \\ M_8(\tilde{\Sigma}) &= \frac{3}{16}\left(35S_1^4 - 120S_1^2S_2 + 96S_1S_3 + 48S_2^2\right), \\ M_{10}(\tilde{\Sigma}) &= \frac{15}{32} \\ &\quad \times \left[63S_1^5 - 280S_1^3S_2 + 240S_1S_2^2 + 48(5S_1^2 - 4S_2)S_3\right], \end{aligned} \tag{91}$$

etc.

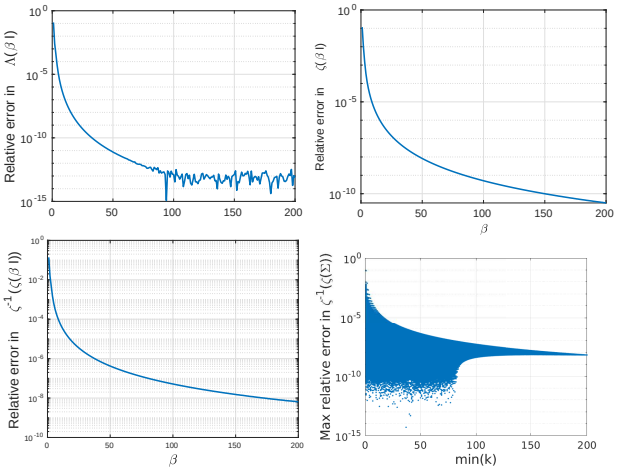

Fig. 4. Accuracy of the approximations. Top left panel: relative error between $\Lambda(\beta\mathbf{I})$ and its approximation, given by Equation (87); Top right panel: relative error of the third order approximation of $\zeta(\beta\mathbf{I})$, given by Equation (108) and the exact values of $\zeta(\beta\mathbf{I})$ as a function of β; Bottom left panel: relative error of the third order inversion $\zeta^{-1}(\mathbf{Z})$, given by Equation (99) for the exact values of $\mathbf{Z} = \zeta(\beta\mathbf{I})$ as a function of β; Bottom right panel: maximum relative error between $\Sigma_{\text{approx}} = \zeta^{-1}[\zeta(\Sigma)]$ and Σ against the minimum values of κ_1, κ_2, κ_3 in the triple, for all combinations of κ_1, κ_2 and κ_3 with values between 1 and 200.

$\Lambda(\Sigma)$ is computable using Equation (87) to any desired accuracy.

If $\Sigma = \beta\mathbf{I}$ and so $\operatorname{Tr}\mathbf{R} = 1 + 2\cos\|\boldsymbol{w}\|$, we have

$$\begin{aligned}\Lambda(\beta\mathbf{I}) &= \int_{\mathcal{SO}(3)} \exp\beta\operatorname{Tr}(\mathbf{R})\,\mathrm{d}\nu(\mathbf{R}) \\ &= \frac{e^{\beta}}{\pi}\int_0^{\pi}(1-\cos\theta)e^{2\beta\cos\theta}d\theta \\ &= e^{\beta}\left(I_0(2\beta) - I_1(2\beta)\right), \end{aligned} \tag{92}$$

where I_0 and I_1 are the zeroth and first order modified Bessel functions respectively. We use this to check the accuracy of the asymptotic approximation; the relative error is shown in the top left panel of Figure 4.

Appendix C. Asymptotic approximations for $\zeta(\Sigma)$ and $\zeta^{-1}(\mathbf{Z})$

In this appendix we derive the asymptotic approximation formulae for $\zeta(\Sigma)$ and $\zeta^{-1}(Z)$. First, we write

$$\begin{aligned}\zeta(\Sigma) &= \frac{\int_{\mathcal{SO}(3)}\mathbf{R}e^{\operatorname{Tr}(\Sigma\mathbf{R})}\,\mathrm{d}\nu(\mathbf{R})}{\int_{\mathcal{SO}(3)}e^{\operatorname{Tr}(\Sigma\mathbf{R})}\,\mathrm{d}\nu(\mathbf{R})} \\ &\sim I + \frac{\sum_{n=0}a_n\int_{\mathbb{R}^3}\|\boldsymbol{y}\|^{2n}\boldsymbol{L}(\boldsymbol{y})^2e^{-\boldsymbol{y}^T\tilde{\Sigma}\boldsymbol{y}}d\boldsymbol{y}}{\sum_{n=0}a_n\int_{\mathbb{R}^3}\|\boldsymbol{y}\|^{2n}e^{-\boldsymbol{y}^T\tilde{\Sigma}\boldsymbol{y}}d\boldsymbol{y}},\end{aligned} \tag{93}$$

where $\tilde{\Sigma}$ is defined in Equation (80), a_n are the coefficients in the Taylor expansion of $1/\sqrt{1-x/2}$ and $\boldsymbol{y} = (y_1, y_2, y_3)^T$. In terms of characteristic functions, we can write $\zeta(\Sigma)$ as

$$\zeta(\Sigma) \sim I - \frac{1}{2}\frac{\sum_{n=0}a_n(-1)^n\frac{\partial^n}{\partial t^n}\det(\mathbf{I}+t\tilde{\Sigma}^{-1})^{-1/2}\Omega(t)\big|_{t=0}}{\sum_{n=0}a_n(-1)^n\frac{\partial^n}{\partial t^n}\det(\mathbf{I}+t\tilde{\Sigma}^{-1})^{-1/2}\big|_{t=0}}, \tag{94}$$

where

$$\Omega(t) = \Omega_1(t) + \Omega_2(t), \tag{95}$$

with

$$\begin{aligned}\Omega_1(t) &= \begin{pmatrix}\frac{1}{\kappa_1+\kappa_3+t} & 0 & 0\\ 0 & \frac{1}{\kappa_1+\kappa_2+t} & 0\\ 0 & 0 & \frac{1}{\kappa_2+\kappa_3+t}\end{pmatrix}, \\ \Omega_2(t) &= \begin{pmatrix}\frac{1}{\kappa_1+\kappa_2+t} & 0 & 0\\ 0 & \frac{1}{\kappa_2+\kappa_3+t} & 0\\ 0 & 0 & \frac{1}{\kappa_1+\kappa_3+t}\end{pmatrix}.\end{aligned} \tag{96}$$

Writing $\Omega_j(0) = \Omega_j$, we see that

$$\frac{\partial^n}{\partial t^n}\Omega_j(t)\big|_{t=0} = (-1)^n n!\Omega_j^{n+1}, \tag{97}$$

It follows that

$$\zeta(\Sigma) \sim I - \frac{1}{2}\frac{\sum_{n=0}a_n\sum_{k=0}^n k!\binom{n}{k}M_{2(n-k)}(\tilde{\Sigma}^{-1})\,(\Omega_1^{k+1}+\Omega_2^{k+1})}{\sum_{n=0}a_nM_{2n}(\tilde{\Sigma}^{-1})}, \tag{98}$$

where the moments M_{2k} are given in Equation (91).

Let ρ denote the operator which cyclically permutes the diagonal of a 3×3 diagonal matrix by shifting one step down the diagonal. In terms of ρ we have

$$\Sigma = \frac{1}{2}\left[\Omega_1^{-1} + \rho^2(\Omega_1^{-1}) - \rho(\Omega_1^{-1})\right], \tag{99}$$

and, for any $k \in \mathbb{Z}$,

$$(\Omega_1^k + \Omega_2^k) + \rho(\Omega_1^k + \Omega_2^k) - \rho^2(\Omega_1^k + \Omega_2^k) = 2\Omega_1^k. \tag{100}$$

Now we transform Equation (98) by defining

$$\mathbf{C} = [\mathbf{I} - \zeta(\Sigma)] + \rho[\mathbf{I} - \zeta(\Sigma)] - \rho^2[\mathbf{I} - \zeta(\Sigma)], \tag{101}$$

where

$$\zeta(\Sigma) = \mathbf{I} - \frac{1}{2}[\rho(\mathbf{C}) + \rho^2(\mathbf{C})]. \tag{102}$$

Using Equation (100) and noting that $M_{2n}(\tilde{\Sigma}^{-1}) = M_{2n}(\Omega_1)$, for all $n \geq 9$, we have

$$\mathbf{C} \sim \frac{\sum_{n=0}a_n\sum_{k=0}^n k!\binom{n}{k}M_{2(n-k)}(\Omega_1)\,\Omega_1^{k+1}}{\sum_{n=0}a_nM_{2n}(\Omega_1)}. \tag{103}$$

To third order, this gives

$$\mathbf{C} \sim \Omega_1 + \frac{1}{4}\Omega_1^2 + \frac{1}{16}\left[3\Omega_1^3 + \operatorname{Tr}(\Omega_1)\Omega_1^2\right] + \cdots. \tag{104}$$

Equation (96)), (104) and (102) in this order provide an algorithm to compute $\zeta(\Sigma)$. Now, to compute ζ^{-1} we look for solutions to Ω_1 of the form

$$\Omega_1 \sim \mathbf{C} + b_1\mathbf{C}^2 + b_2\mathbf{C}^3 + b_3\operatorname{Tr}(\mathbf{C})\mathbf{C}^2 + \cdots. \tag{105}$$

This gives,

$$\begin{aligned}\Omega_1 &+ \frac{1}{4}\Omega_1^2 + \frac{1}{16}\left[3\Omega_1^3 + \operatorname{Tr}(\Omega_1)\Omega_1^2\right] \\ &= \mathbf{C} + (b_1+1/4)\mathbf{C}^2 + (b_2 - b_1/2 + 3/16)\mathbf{C}^3 \\ &\quad + (b_3 + 1/16)\operatorname{Tr}(\mathbf{C})\mathbf{C}^2 + \cdots.\end{aligned} \tag{106}$$

Choice of $b_1 = -1/4$, $b_2 = -1/16$ and $b_3 = -1/16$ gives the approximate inversion

$$\Omega_1 \sim \mathbf{C} - \frac{1}{4}\mathbf{C}^2 - \frac{1}{16}\left[\mathbf{C}^3 + \operatorname{Tr}(\mathbf{C})\mathbf{C}^2\right] + \cdots. \tag{107}$$

This is then substituted in Equation (99) to recover Σ. With some work, higher order terms can be calculated if necessary.

This is an asymptotic series (it does necessarily converge) and one maximises accuracy by only summing to the term before the smallest magnitude term. The bottom right panel in Figure 4 shows the maximum relative error between $\Sigma_{\text{approx}} = \zeta^{-1}[\zeta(\Sigma)]$ and Σ against the minimum values of κ_1, κ_2, κ_3 for all combinations of κ_1, κ_2 and κ_3 with values between 3 and 200. This is done by computing $\zeta(\Sigma)$ to third order and then using Equation (107). The approximation is better (and, in fact, almost exact) for larger values of κ_is. If $\Sigma = \beta\mathbf{I}$ the $\zeta(\Sigma)$ can be calculated exactly in terms of modified Bessel functions, denoted by I_0, I_1 and I_2, for zeroth,first and second order respectively, as

$$\zeta(\beta\mathbf{I}) = \left[1 - \frac{1}{3}\frac{3I_0(2\beta) - 4I_1(2\beta) + I_2(2\beta)}{I_0(2\beta) - I_1(2\beta)}\right]\mathbf{I}. \quad (108)$$

The top right panel in Figure 4 shows the accuracy of this approximation in terms of relative error between computed and exact values of $\zeta(\beta\mathbf{I})$. The bottom left panel in Figure 4 shows the accuracy of the third order inversion for these values of $\zeta(\beta\mathbf{I})$.

Appendix D. Taylor expansion of $\text{Tr}\left(\mathbf{B}\mathbf{R}_{\boldsymbol{w}_0}^T d\mathbf{R}_{\boldsymbol{w}}\right)$

Here, we compute the second order Taylor expansion of $\text{Tr}\left(\mathbf{B}\mathbf{R}_{\boldsymbol{w}_0}^T d\mathbf{R}_{\boldsymbol{w}}\right)$ in terms of $\boldsymbol{w}$ at $\boldsymbol{w}_0$. First, note that the first term of the Taylor expansion vanishes

$$\text{Tr}\left(\mathbf{B}\mathbf{R}_{\boldsymbol{w}_0}^T d\mathbf{R}_{\boldsymbol{w}}\right)\Big|_{\boldsymbol{w}=\boldsymbol{w}_0} = \text{Tr}\left[\mathbf{B}\boldsymbol{L}\left(\mathbf{G}_{\boldsymbol{w}_0} d\boldsymbol{w}_0\right)\right] = 0, \quad (109)$$

since $\mathbf{B}$ is symmetric and $\boldsymbol{L}\left(\mathbf{G}_{\boldsymbol{w}_0} d\boldsymbol{w}_0\right)$ is anti-symmetric; $\boldsymbol{L}$ is defined in Equation (61), and the matrix $\mathbf{G}_{\boldsymbol{w}_0}$ is computed in Equation (70). For the second term we calculate

$$\begin{aligned}\mathbf{R}_{\boldsymbol{w}}^T \frac{\partial^2 \mathbf{R}_{\boldsymbol{w}}}{\partial w_\ell \partial w_j} = &\sum_m \left\{\frac{\partial \mathbf{G}_{\boldsymbol{w}}}{\partial w_\ell}\right\}_{mj} L_m \\ &+ \sum_{mm'} \{\mathbf{G}_{\boldsymbol{w}}\}_{mj}\{\mathbf{G}_{\boldsymbol{w}}\}_{m'\ell} L_{m'} L_m,\end{aligned} \quad (110)$$

where L_j's for $j = 1, \ldots, 3$ are defined in Equation (62). Next

$$\text{Tr}\left(\mathbf{B}\mathbf{R}_{\boldsymbol{w}}^T \frac{\partial^2 \mathbf{R}_{\boldsymbol{w}}}{\partial w_\ell \partial w_j}\right) = \sum_{m'm} \{\mathbf{G}_{\boldsymbol{w}}\}_{mj}\{\mathbf{G}_{\boldsymbol{w}}\}_{m'\ell}\, \text{Tr}(\mathbf{B}L_{m'}L_m), \quad (111)$$

since $\text{Tr}(\mathbf{B}L_j) = 0$ for $j = 1, \ldots, 3$. The expression $\text{Tr}(\mathbf{B}L_mL_i)$ defines elements of a matrix $\tilde{\mathbf{B}}$ as

$$\{\tilde{\mathbf{B}}\}_{im} = \text{Tr}(\mathbf{B}L_mL_i). \quad (112)$$